European Radiology (2020) 30:3083–3093
https://doi.org/10.1007/s00330-019-06515-y

ONCOLOGY

Shortening the acquisition time of whole-body MRI: 3D T1 gradient echo Dixon vs fast spin echo for metastatic screening in prostate cancer

Frédéric E. Lecouvet[1] · Vassiliki Pasoglou[1] · Sandy Van Nieuwenhove[1] · Thomas Van Haver[1] · Quentin de Broqueville[1] · Vincent Denolin[2] · Perrine Triqueneaux[1] · Bertrand Tombal[1] · Nicolas Michoux[1]

Received: 21 July 2019 / Revised: 30 September 2019 / Accepted: 15 October 2019 / Published online: 17 February 2020

Abstract

Purpose To compare 3D T1-weighted fast spin echo (FSE) and 3D T1-weighted gradient echo (GE) mDixon as morphologic sequences to complement diffusion-weighted imaging (DWI) for the metastatic screening in prostate cancer (PCa) patients.

Materials and methods Thirty PCa patients at high risk of metastases prospectively underwent both a 3D T1 FSE (14 min) and a rapid 3D T1 GE^{mDixon} (1 min 20 s) sequences within a WB-MRI protocol. Two readers assessed the diagnostic performance of the FSE/Fat/in-phase (IP)/IP+Fat sequences in detecting bone and node metastases. The reference standard was established by a panel of four physicians on the basis of all baseline and follow-up imaging, biological and clinical information. The reproducibility of readings, predictive accuracy (Acc) from ROC curves analysis, and contrast-to-reference ratio (CRR) in lesions were assessed for each sequence.

Results In bone and lymph nodes (per-region analysis), reproducibility was at least good for all sequences/readers, except for nodes in the common iliac/inguinal regions. In bone (per-organ analysis), Acc of FSE was superior to that of mDixon (difference + 4%, $p < 0.0083$). In nodes (per-organ analysis), Acc of Fat was superior to that of other sequences (difference + 4% to + 6% depending on reader, $p < 0.0083$). In the per-patient analysis, Acc of FSE was superior to that of mDixon (difference + 4% to + 6% depending on sequence, $p < 0.0083$). Fat images had higher CRR compared with FSE in the thoracic spine, the bony pelvis and lymph node metastases ($p < 0.025$).

Conclusion 3D T1 GE^{mDixon} may replace 3D T1 FSE to complement DWI in WB-MRI for metastatic screening in PCa. It demonstrates an Acc ranging from + 4% to + 6% (nodes) to − 4% to − 6% (bone and patient staging) compared with FSE and considerably reduces the examination time, offering the perspective of acquiring WB-MRI examinations in less than 20 min.

Key Points

- *The replacement of 3D T1 FSE by the 3D T1 GE mDixon as morphologic sequence to complement DWI drastically reduces the acquisition time of WB-MRI studies.*
- *The 3D T1 GE mDixon sequence offers similar reproducibility of image readings compared with that of the 3D T1 FSE.*
- *Differences in diagnostic accuracy are limited (+ 4%/+ 6% in favor of mDixon to detect node metastases; + 4%/+ 6% in favor of FSE to detect bone metastases/metastatic disease in a patient).*

Electronic supplementary material The online version of this article (https://doi.org/10.1007/s00330-019-06515-y) contains supplementary material, which is available to authorized users.

✉ Frédéric E. Lecouvet
frederic.lecouvet@uclouvain.be

[1] Department of Radiology an Medical Imaging, Centre du Cancer and Institut de Recherche Expérimentale et Clinique (IREC), Cliniques Universitaires Saint-Luc, Université Catholique de Louvain (UCLouvain), Avenue Hippocrate 10/2942, B-1200 Brussels, Belgium

[2] Philips Medical Systems International BV, Veenpluis 4-6, 5684 PC Best, The Netherlands

Keywords Magnetic resonance imaging · Whole-body imaging · Neoplasm metastasis · Prostate · Bones

Abbreviations

Acc	Predictive accuracy
ADC	Apparent diffusion coefficient
AUC	Area under the receiver operating characteristic curve
BCR	Biochemical recurrence
BS	Bone scintigraphy
BVC	Best valuable comparator
CI	Confidence interval
CRPC	Castrate-resistant prostate cancer
CRR	Contrast-to-reference ratio
DWI	Diffusion-weighted imaging
DWIBS	DWI with background signal suppression
FSE	Fast spin echo
GE	Gradient echo
IP	In-phase
IR	Inversion recovery
ND	Newly diagnosed
OP	Out-phase
PACS	Picture Archiving and Communication System
PCa	Prostate cancer
PET	Positron emission tomography
PSA	Prostate-specific antigen
ROC	Receiver operating characteristic
ROI	Region of interest
STIR	Short tau inversion recovery

Introduction

WB-MRI has emerged as an effective alternative to older diagnostic modalities such as bone scintigraphy (BS) and thoraco-abdomino-pelvic CT for bone, node and visceral staging in prostate cancer (PCa) [1–5]. The number of indications of WB-MRI is growing in solid and hematologic cancers such as multiple myeloma and lymphoma [2, 6]. However, its use in oncology is hampered by its acquisition times, often superior to 30 min, facing limited magnet availability. Anatomic and diffusion-weighted imaging (DWI) sequences both account for approximately 50% of WB-MRI acquisition time. The acquisition of anatomic 3D sequences with small (almost) isotropic voxels has been proposed as a substitute to the repetition of 2D images with similar contrasts obtained in different planes [4, 5]. A 3D T1 fast spin echo (FSE) sequence may be performed as anatomic sequence, providing a diagnostic performance that is equal or superior to the sum of 2D sequences obtained in several planes for the detection of bone and node metastases [5].

A faster alternative to FSE may consist in a 3D T1–modified Dixon (mDixon) gradient echo (GE) acquisition. The T1 GE^{mDixon} provides images with different contrasts automatically derived from the acquisition, i.e., in-phase (IP), out-phase (OP), Fat, and Water images [7–10]. These 3D T1 FSE and GE^{mDixon} sequences have been suggested as sufficient anatomical counterparts of DWI in WB-MRI performed to detect bone and node metastases in PCa [8, 11]. Larbi et al showed that the diagnostic effectiveness of FSE+DWI was not improved by the addition of a coronal STIR acquisition covering the body [11]. Johnston et al showed that the effectiveness of GE^{mDixon}+DWI was not improved by the addition of a T2-weighted and post-contrast T1 mDixon acquisitions covering the body [8]. There is no data in the literature comparing the 3D T1 FSE versus GE^{mDixon} in WB-MRI [12, 13]. This prospective study compares these sequences in terms of reproducibility of readings, predictive accuracy for the detection of bone and node metastases, and contrast resolution.

Materials and methods

Patients

This prospective study was approved by the institutional ethics committee. Written informed consent was obtained from all patients. The study is listed on ClinicalTrials.gov under the identifier NCT03034070. It included consecutive PCa patients referred by the Department of Urology for metastatic screening because of high risk of metastasis. Patients were considered at high risk of metastases whenever they presented one of the following features: for ND, clinical stage ≥ T3a, Gleason score ≥ 8, prostate-specific antigen (PSA) > 20 ng/mL [14–16]; for BCR after radical prostatectomy, 2 consecutive measurements of PSA ≥ 0.2 ng/mL; and for BCR after primary radiation, PSA nadir + 2; for CRPC, increasing PSA level > 8 ng/mL while receiving androgen deprivation therapy with a PSA doubling time < 10 months.

MR imaging

Patients were imaged on a 3.0-T MR magnet (Ingenia, Philips Healthcare) in the supine position and were covered with a head and neck coil and two anterior coils, combined with the table-embedded posterior coils. A WB-MRI protocol including (at least) an isotropic free-breathing 3D T1 FSE sequence, a breath-hold 3D T1 GE^{mDixon} sequence, and a free-breathing DWI sequence was then performed. All sequences covered the body from the vertex to midthighs in 4 stacks.

The FSE sequence was adapted from published work [5]. The GE^{mDixon} was based on a modified 2-point Dixon scheme (mDixon FFE) which allows for divergences from exact in-phase (IP) and out-phase (OP) echo times (TE) and therefore

offers maximum flexibility in protocol optimization [17]. Synthetic Water, Fat, IP, and OP images were reconstructed from the mDixon acquisition. The in-plane acquisition resolution of the GE^{mDixon} (1.5 mm × 1.5 mm) was close to that of the FSE (1.14 mm × 1.3 mm), although the slice thickness had to be larger (3 mm versus 1.2 mm) to allow breath-hold acquisitions at the thoraco-abdominal levels. Those 3D T1 sequences were acquired in the coronal plane. DWI was performed in the transverse plane using a DWIBS (DWI with background signal suppression) acquisition based on a transversal inversion recovery (IR) spin echo echo-planar sequence (DWI IR SE-EPI) using 4 *b* values. DWIBS images were reformatted in the coronal plane for side-by-side (stitched) analysis with the 3D T1 sequences. Acquisition parameters are summarized in Table 1. The total acquisition time of the 3 sequences was 31.8 min. Additional optional sequences (coronal STIR and transverse T2 FSE sequences) were not considered for the present study.

MRI readings

Images from FSE, IP, Fat, and all (= IP+Fat, i.e., both reconstructed images being available and read together by the observer) sequences were assessed twice by two radiologists with 3-year and 8-year experience, using multiplanar reformation, windowing and zooming tools of the Picture Archiving and Communication System (PACS) (Carestream Vue; Carestream Health). Assessments were independent, blinded to clinical information, randomized with at minimum a 4-week interval between readings. Water and OP images derived from the GE^{mDixon} were not considered for analysis based on previous evaluation of their limited diagnostic interest [7, 18]. No other sequence (DWI in particular, left for the adjudication within the best valuable comparator, see below) was available by the time of this reading.

During each reading, the metastatic assessment was conducted as follows. Firstly, the presence, location, and number of metastases were determined in each anatomic region (per-region analysis). Secondly, the metastatic status (positive if at least one region of the organ was positive) was determined for each of the 2 organs, bone and lymph nodes (per-organ analysis). Thirdly, the metastatic status of each patient (positive if at least one organ was positive) was determined (per-patient analysis).

Eight anatomical regions for bones (skull, thoracic cage, cervical spine, thoracic spine, lumbar spine, pelvis, humeri, femurs) and seven regions for nodes (inguinal, internal and external iliac together, common iliac, lumbo-aortic, thoracic, axillary, cervical regions) were studied for the metastatic assessment.

For bone lesions, a focal metastasis was defined as a rounded focus larger than 5 mm with low signal intensity on T1-weighted images and, for the evaluation of the whole examination, of low signal intensity on T1 and high signal intensity on the high *b* value DWI sequence. Diffuse bone metastasis was defined as low signal intensity of the bone marrow (lower than the signal intensity of disks and muscles) on T1-weighted images and, for the evaluation of the whole examination, of low signal intensity on T1 and high signal intensity on the high *b* value DWI sequence.

Lymph nodes were considered abnormal when their short-axis diameter was larger than 10 mm. Perivisceral (perirectal, etc.) nodes were defined as abnormal when their short-axis

Table 1 MRI sequence parameters

	3D T1 FSE	3D T1 GE mDixon	DWIBS
Acquisition time	4 × 4 min 30 s	4 × 20.5 s	4 × 3 min 36 s
Scan orientation	Coronal	Coronal	Axial
Phase-encoding direction	Feet–head	Right–left	Anterior–posterior
Acquired voxel size (mm) (read × phase × slice)	1.14 × 1.30 × 1.20	1.50 × 1.50 × 3.00	4.4 × 4.8 × 6
Field of view (mm) (read × phase × slice)	500 × 300 × 252	300 × 450 × 230	440 × 348 × 305
Acquisition matrix (read × phase × slice)	440 × 230 × 210	200 × 299 × 153	100 × 74 × 50
No. of stations	4	4	4
Overlap between stations (mm)	50	50	50
Coverage in *z*-axis (mm)	1050	1050	1070
SENSE factor (phase × slice)	1.7 × 2.5	3.5 × 2	3 × 1
Phase oversampling (mm)	200 H, 200 F	103 R, 103 L	0
TR/TE (ms)	285/21	3.8/1.46, 2.6	6000/59 (TI, 250 ms)
No. of signals acquired	2	1	5
Turbo factor	50	NA	NA
Flip angle (degrees)	90	10	130
Bandwidth (Hz)	1114	1953	255
Fat suppression technique	–	–	STIR
Specific parameters	–	–	*b* values 0, 50, 150, 1080

was larger than 8 mm. Lymph nodes were also considered abnormal when their contours were irregular or when their normal kidney shape and/or the fatty hilum was absent.

Image quality

Signal-to-noise ratio and contrast-to-noise ratio were not calculated, as the standard deviation of noise could not be measured due to automatic thresholding of the image background to zero on the saved data of the mDixon sequences. As the value of a sequence used for lesion detection mainly relies, beside spatial resolution and signal-to-noise ratio, on the contrast provided by this sequence between lesions and their environment, a contrast-to-reference ratio (CRR) (i.e., a lesion to background ratio) was assessed using the equation: CRR = $S^{\text{lesion}}/S^{\text{reference}}$, where S^{lesion} is the mean signal intensity in the lesion (skeletal or nodal) and $S^{\text{reference}}$ is the mean signal intensity in the reference tissue (Figs. 1 and 2). As metastases have low signal intensity and reference fatty tissue has high signal intensity on T1-weighted MR images, a lower CRR value indicates a higher contrast between lesion and reference tissue. Measurements were performed by one radiologist (TVH) after validation of the true pathologic nature of the measured lesions (according to the BVC). A single ROI, the largest possible without including bone cortices and anatomic margins of lymph nodes, was delineated in each metastatic region. For spine lesions, the reference ROI was chosen in an unequivocally non-metastatic bone marrow area of the metastatic vertebra or, if impossible, in the bone marrow of the closest uninvolved vertebra. For pelvic bone lesions, the reference ROI was chosen in an unequivocally non-metastatic bone marrow area. For lymph nodes, the reference ROI was chosen in the local-regional fat. Lesions in regions with artifacts, bone lesions with ambiguous T1 signal (suggestive of fracture, scar tissue, or benign conditions), regions of fatty marrow conversion due to radiotherapy, and diffuse bone metastasis were not considered for these measurements.

Statistical analysis

Calculations were done with Medcalc Statistical Software (https://www.medcalc.org/) and Matlab (Matlab R2017a, MathWorks).

Reproducibility of MRI readings

Inter-observer agreement was assessed for each MRI sequence in the per-region analysis according to Scott's pi [19]. The strength of agreement was interpreted according to the Altman's scale as follows: $pi < 0.20$ = poor; $0.21 \leq pi < 0.40$ = fair; $0.41 \leq pi < 0.60$ = moderate; $0.61 \leq pi < 0.80$ = good ; and $pi \geq 0.81$ = very good.

Diagnostic performance

In the absence of a systematic histopathological gold standard, a best valuable comparator (BVC) was used as the reference standard to assess the diagnostic performance of the sequences [20, 21]. The two readers, along with a third radiologist with 12-year experience in WB-MRI reading and one oncologist, established the BVC defining the metastatic status in each region, organ, and patient. This assignment was based on the

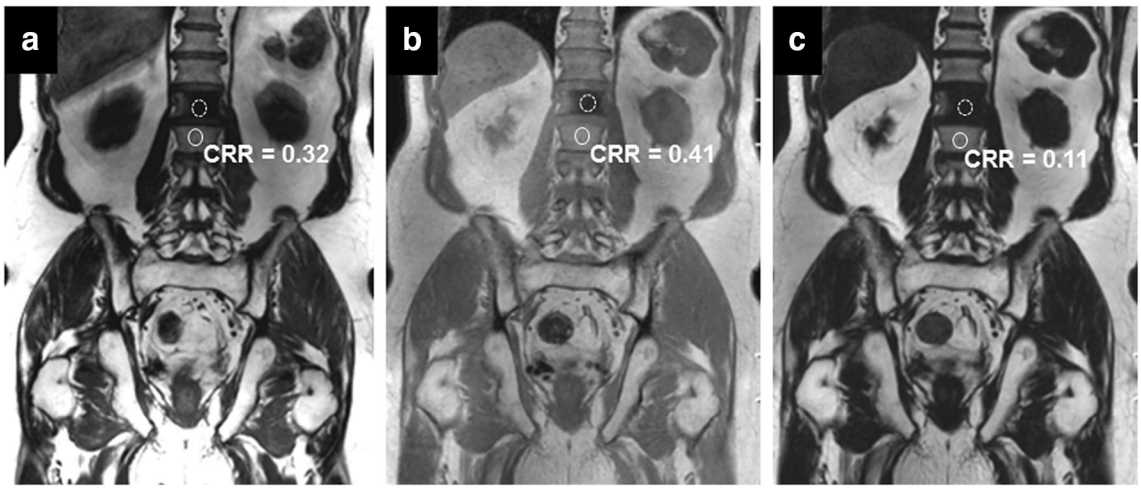

Fig. 1 Measurement of the contrast-to-reference ratio (CRR) in a bone metastasis. Coronal reformatted 3D T1-weighted sequences from WB-MRI study in a 66-year-old patient with newly diagnosed prostate cancer illustrate measurements of CRR in a L1-vertebral body metastasis on FSE (**a**), IP GE (**b**), and Fat GE (**c**) images. The largest possible region of interest (ROI) that fits the bone lesion is chosen (dotted circle), without including the bone cortices. The reference ROI (circle) is chosen in an unequivocally non-metastatic bone marrow area (adjacent uninvolved L2 vertebral body). The lowest CRR (highest contrast between lesion and reference tissue) is obtained for the Fat image, followed by the FSE image and by the IP image

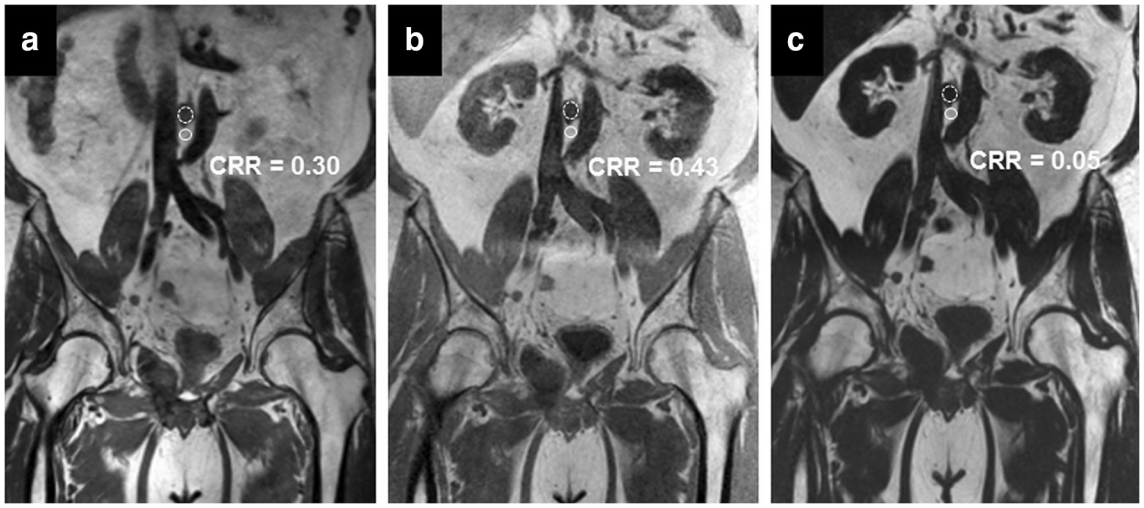

Fig. 2 Measurement of the CRR in a node metastasis. Coronal reformatted 3D T1-weighted sequences from WB-MRI study in a 60-year-old patient with newly diagnosed prostate cancer illustrate measurements of CRR in a lumbo-aortic lymph node on FSE (**a**), IP GE (**b**), and fat GE (**c**) images. The largest possible region of interest (ROI) that fits the node lesion is chosen (dotted circle), without including the anatomic margins of the lymph node. The reference ROI (circle) is chosen in the local-regional Fat. The lowest CRR (highest contrast between lesion and reference tissue) is obtained for the Fat image, followed by the FSE image and by the IP image

panel review of the following: (i) the patients' complete WB-MRI study (FSE, GE^{mDixon}, DWI, optional sequences); (ii) the imaging follow-up (≥ 6 months) and other imaging modalities (BS, thoraco-abdomino-pelvic CT scan available in all patients, and prostate-specific membrane antigen (PSMA)–ligand positron emission tomography (PET) available in 18 out of 30 patients); and (iii) all baseline and follow-up clinical and biological results.

Receiver operating characteristic (ROC) curves analysis was performed to assess the diagnostic performance of the sequences in the per-region, per-organ, and per-patient analyses [22]. A p value < 0.05 was regarded as statistically significant. To assess the differences in predictive accuracy (Acc) between sequences, a resampling procedure without replacement based on 300 samples of $N = 25$ patients randomly drawn from the whole cohort of patients was performed. Then, a Wilcoxon test was performed from which the median difference in Acc between sequences was derived. Due to the multiple comparisons that were performed between MRI sequences, a Bonferroni-like correction was applied. A p value < 0.0083 was thus regarded as statistically significant for this latter test [23].

Image quality

Due to the non-normality of the data distribution (according to the Shapiro-Wilk test at $p < 0.05$), CRRs were compared between MRI sequences using an analysis of variance (Kruskal-Wallis test at $p < 0.05$) followed by a Wilcoxon test (at $p < 0.025$). This analysis was performed in the pelvic, in the spinal and femoral bone lesions, and in the lymph nodes. These tests were not performed in other regions due to the low prevalence of positive lesions.

Results

Patient population

Thirty consecutive PCa patients at high risk of metastases were prospectively enrolled between September 2017 and January 2018. The mean patient age (± standard deviation) was 70.6 ± 7.1 years (range, 56–85 years). The PSA levels' range was 22–615 (median, 97) ng/mL in ND; 0.2–20.5 (median, 2.4) ng/mL in BCR; and 1.98–23 (median, 2.7) ng/mL in CRPC. According to the BVC, 21 patients had one ($n = 4$) or more bone metastases; 16 had one ($n = 4$) or more node metastases; and 13 patients had both bone and node metastases. Table 2 illustrates the prevalence of lesions in the patient groups based on disease stage.

Table 2 Patients' characteristics: distribution of metastatic disease in bones and lymph nodes according to disease stage in 30 PCa patients

Patients		Bone metastases			Node metastases	
Characteristics	*N*	Absent	Diffuse	Focal	Absent	Present
ND	9	4	2	3	6	3
BCR	15	4	2	9	5	10
CRPC	6	1	3	2	3	3
Total	30	9	7	14	14	16

ND, newly diagnosed; *BCR*, biochemical recurrence; *CRPC*, castration-resistant PCa; *N*, number

Reproducibility of MRI readings

Inter-observer agreement in the per-region analysis is reported in Table 3. In bone, the reproducibility of FSE ranged from good to very good, while it ranged from poor to very good in nodes. The reproducibility of IP ranged from moderate to very good in bone, while it ranged from poor to very good in nodes. The reproducibility of Fat ranged from good to very good in bone, while it ranged from poor to very good in nodes. The reproducibility of IP+Fat ranged from good to very good in bone, while it ranged from poor to very good in nodes. Figures 3 and 4 show examples of discrepancies in readings between the FSE and mDixon sequences.

Diagnostic performance

Results from the ROC curves analysis in the per-organ and per-patient analyses are reported in Table 4. Comparison of Acc is reported in Table 5. Results from the ROC curves analysis in the per-region analysis are provided in supplementary Tables A-D.

In bone (per-organ analysis), Acc of FSE was higher than or equal to that of mDixon sequences for both readers. The gain in accuracy was small (median difference of + 4% compared with mDixon). In nodes (per-organ), Acc of Fat was higher than or equal to that of FSE for both readers. The gain in accuracy was small (median difference ranging from + 4% to + 6% depending on the reader).

In the per-patient analysis, Acc of FSE was higher than or equal to that of mDixon sequences for both readers. The gain in accuracy was small (median difference ranging from + 4% to + 6% compared with mDixon).

Image quality

Forty focal bone and 18 node metastases were analyzed. In total, 116 ROIs were defined on each sequence (58 lesions + 58 reference areas) (Figs. 1 and 2). CRR values are reported in Table 6. A significantly lower CRR was observed on Fat images compared with that on FSE images in pelvic bone lesions and in lymph node metastases. A lower CRR was also observed on Fat images in other skeletal areas but without reaching statistical significance.

Discussion

WB-MRI has gained acceptance as a screening tool in patients with metastases from solid cancers and hematologic malignancies [2, 4, 24]. However, cost and long acquisition times are barriers for its use in clinical routine. A faster alternative to the 3D T1 FSE sequence in WB-MRI may consist in the use of the 3D T1 GE^{mDixon}. Limited information exists on the comparison of these sequences. Published studies have focused on peripheral joints and on the comparison in the quality of fat suppression between mDixon and FSE sequences [25, 26]. In a recent retrospective study focusing on the pelvis, Samji et al compared the diagnostic performances of a 2-point Dixon T1 FSE sequence and of a 3D T1 GE sequence in patients undergoing pre-treatment PCa staging, showing that the GE^{mDixon} had a similar or higher performance

Table 3 Reproducibility of MRI readings in the per-region analysis

Anatomic area	FSE	IP	Fat	All (IP + Fat)
Skull	0.61 (0.18; 0.86)	0.42 (0.04; 0.76)	0.75 (0.32; 0.93)	0.90 (0.54; 0.98)
Thorax	0.80 (0.49; 0.93)	0.79 (0.48; 0.93)	0.63 (0.27; 0.84)	0.87 (0.57; 0.96)
Cervical spine	0.66 (0.28; 0.86)	0.81 (0.44; 0.95)	0.91 (0.57; 0.98)	1.00 (0.72; 1.00)
Thoracic spine	0.79 (0.48; 0.93)	0.93 (0.67; 0.99)	0.79 (0.46; 0.93)	0.79 (0.48; 0.93)
Lumbar spine	0.93 (0.66; 0.99)	0.93 (0.67; 0.99)	0.78 (0.45; 0.92)	0.87 (0.57; 0.96)
Pelvis	0.78 (0.45; 0.92)	0.80 (0.48; 0.93)	0.86 (0.55; 0.96)	0.93 (0.66; 0.99)
Humeri	0.79 (0.39; 0.94)	1.00 (0.63; 1.00)	0.87 (0.43; 0.98)	0.89 (0.50; 0.98)
Femurs	0.78 (0.45; 0.92)	0.92 (0.62; 0.99)	0.75 (0.40; 0.91)	0.85 (0.53; 0.96)
Int-ext iliac	1.00 (0.67; 1.00)	0.76 (0.33; 0.93)	0.67 (0.25; 0.88)	1.00 (0.67; 1.00)
Common iliac	0.52 (0.11; 0.80)	− 0.05 (− 0.05; 0.59)	0.35 (− 0.005; 0.76)	1.00 (0.22; 1.00)
Lumbo-aortic	0.91 (0.58; 0.98)	0.81 (0.44; 0.95)	0.90 (0.54; 0.98)	0.76 (0.33; 0.93)
Inguinal	0.46 (0.04; 0.85)	0.65 (0.10; 0.94)	− 0.03 (− 0.03; 0.68)	0.65 (0.10; 0.94)
Thoracic	0.84 (0.35; 0.97)	0.84 (0.35; 0.97)	0.63 (0.15; 0.90)	0.78 (0.24; 0.96)
Axillary	1.00 (0.22; 1.00)	1.00 (0.22; 1.00)	1.00 (0.22; 1.00)	1.00 (0.22; 1.00)
Cervical	− 0.03 (− 0.03; 0.68)	− 0.03 (− 0.03; 0.68)	NC	− 0.03 (− 0.03; 0.68)

Agreement according to the Scott's *pi* (*pi*) (and its 95% confidence interval) is given. Note that the $pi \leq 0.1$ observed and the non-computable (NC) case result from the low prevalence of positive lesions in the corresponding anatomical regions

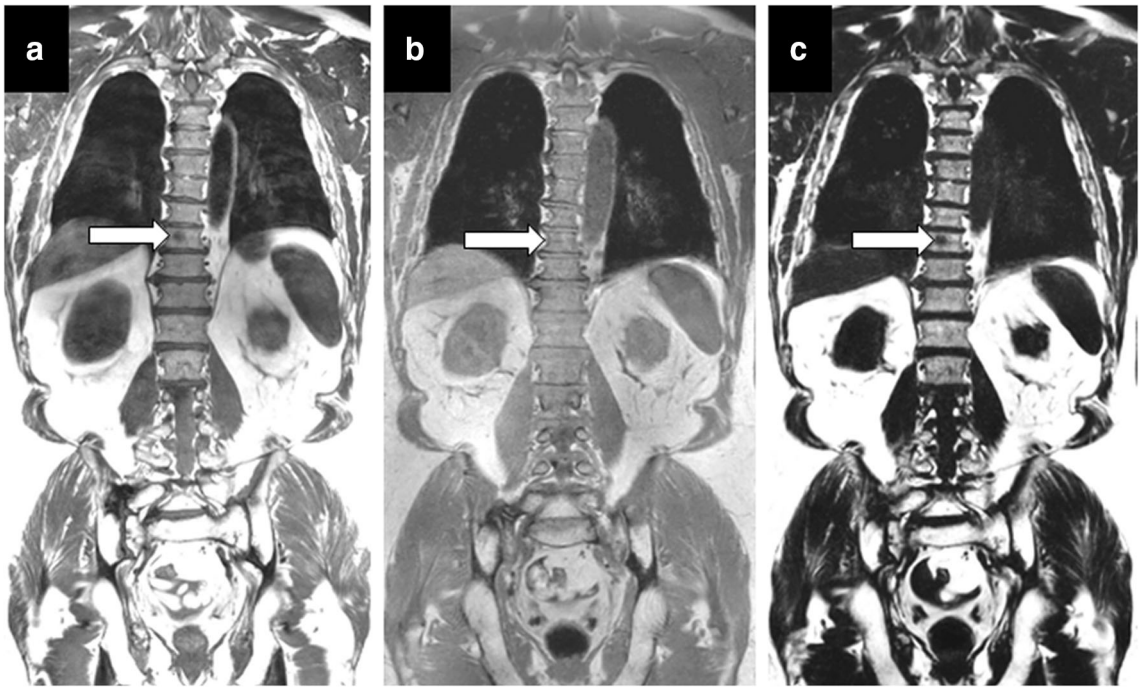

Fig. 3 Example of discrepancies in readings of the different sequences. Coronal reformatted 3D T1-weighted sequences from WB-MRI study in a 77-year-old patient with metastatic castrate-resistant prostate cancer illustrate the presence of a bone metastasis within the T9 vertebral body. 3D T1 FSE (**a**) shows bone metastasis (arrow in **a**), which was missed by the reader on the 3D T1 GE in-phase image (arrow in **b**), but was evident on the 3D T1 GE Fat image (arrow in **c**)

compared with that of FSE for the detection of bone and node metastases, while reducing the acquisition time from 5 min 16 s to 2 min 37 s [27].

Our prospective study comparing 3D T1 GE^{mDixon} and 3D T1 FSE sequences for metastatic screening in PCa patients had the following results.

Firstly, our results showed that, in bone (per-region), the reproducibility of the readings was at least good for each sequence and reader (except in the skull where the reproducibility of IP was moderate only). In nodes (per-region), the reproducibility was also at least good for each sequence and reader (except in the common iliac, inguinal, and cervical regions where the prevalence of lesions was very low). The reproducibility of combined IP+Fat readings was very good, probably resulting from the maximization of the information provided by the availability of 2 sequences.

Secondly, our study showed that, in bones (per-organ), the predictive accuracy of FSE was significantly higher than that of IP and equivalent or higher to that of Fat and IP+Fat, depending on the reader. This superiority of FSE may theoretically result from a higher spatial resolution of the sequence, or from a more nuanced contrast due to wider distribution of pixel intensities compared with the sharper contrast of Fat or lower contrast of IP images. In nodes (per-organ), Acc of Fat was significantly higher than that of FSE and IP, while the accuracy of IP was equivalent or higher than that of FSE depending on the reader. The lower accuracy of FSE may result from the proximity of lymph nodes not only with the vessels but also with the bowel, which can induce motion artifacts. Motion artifacts are reduced on mDixon images due to much shorter acquisition time enabling breath-holding, explaining their use in abdominal MRI protocols.

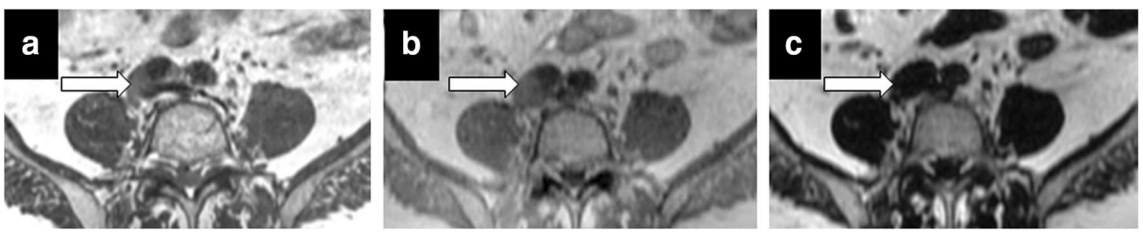

Fig. 4 Example of discrepancies in readings of the different sequences. Transverse 3D T1-weighted sequences from WB-MRI study in a 73-year-old patient with metastatic castrate resistant prostate cancer illustrate the presence of a right iliac node metastasis. 3D T1 FSE (**a**) shows abnormal lymph node (arrow in **a**), which was also detected by the reader on the 3D T1 GE in-phase image (arrow in **b**), but was missed on the 3D T1 GE Fat image, due to its very low signal intensity which was similar to that of the adjacent vessels (arrow in **c**). Despite this false-negative observation, the 3D T1 GE Fat was superior to the other sequences for abnormal lymph node detection in the global study population

Table 4 Diagnostic performance of MRI sequences in detecting bone and node metastases in the per-organ (bone and nodes) and per-patient analysis

	Se (%)	Sp (%)	PPV (%)	NPV (%)	Acc (%)	AUC	*p* value
FSE							
Bone	95 (76; 100)	67 (30; 93)	87 (66; 97)	86 (42; 100)	87	0.810	0.0004
	100 (84; 100)	*89 (52; 100)*	*96 (77; 100)*	*100 (63; 100)*	*97*	*0.944*	*< 0.001*
Nodes	81 (54; 96)	93 (66; 100)	93 (66; 100)	81 (54; 96)	87	0.871	< 0.0001
	81 (54; 96)	*100 (77; 100)*	*100 (75; 100)*	*82 (57; 96)*	*90*	*0.906*	*< 0.0001*
Per-patient	100 (86; 100)	67 (22; 96)	92 (75; 99)	100 (29; 100)	93	0.833	0.0016
	100 (86; 100)	*83 (36; 100)*	*96 (80; 100)*	*100 (39; 100)*	*97*	*0.917*	*< 0.0001*
IP							
Bone	90 (70; 99)	67 (30; 93)	86 (65; 97)	75 (35; 97)	83	0.786	0.0014
	95 (76; 100)	*89 (52; 100)*	*95 (76; 100)*	*89 (52; 100)*	*93*	*0.921*	*< 0.0001*
Nodes	88 (62; 98)	93 (66; 100)	93 (68; 100)	87 (60; 98)	90	0.902	< 0.0001
	88 (62; 98)	*93 (66; 100)*	*93 (68; 100)*	*87 (60; 98)*	*90*	*0.902*	*< 0.0001*
Per-patient	96 (79; 100)	50 (12; 88)	89 (70; 98)	75 (13; 100)	87	0.729	0.0439
	96 (79; 100)	*67 (22; 96)*	*92 (74; 99)*	*80 (23; 100)*	*90*	*0.812*	*0.0036*
Fat							
Bone	100 (84; 100)	56 (21; 86)	84 (64; 96)	100 (48; 100)	87	0.778	0.0016
	95 (76; 100)	*89 (52; 100)*	*95 (76; 100)*	*89 (52; 100)*	*93*	*0.921*	*< 0.0001*
Nodes	88 (62; 98)	100 (77; 100)	100 (77; 100)	88 (62; 98)	93	0.937	< 0.0001
	88 (62; 98)	*100 (77; 100)*	*100 (77; 100)*	*88 (62; 98)*	*93*	*0.937*	*< 0.0001*
Per-patient	100 (86; 100)	50 (12; 88)	89 (71; 98)	100 (16; 100)	90	0.750	0.0253
	96 (79; 100)	*83 (36; 100)*	*96 (79; 100)*	*83 (31; 100)*	*93*	*0.896*	*< 0.0001*
All (IP+Fat)							
Bone	100 (84; 100)	56 (21; 86)	84 (64; 96)	100 (48; 100)	87	0.778	0.0016
	100 (84; 100)	*78 (40; 97)*	*91 (72; 99)*	*100 (59; 100)*	*93*	*0.889*	*< 0.0001*
Nodes	88 (62; 98)	100 (77; 100)	100 (77; 100)	88 (62; 98)	93	0.937	< 0.0001
	69 (41; 89)	*93 (66; 100)*	*92 (62; 100)*	*72 (47; 90)*	*80*	*0.808*	*< 0.0001*
Per-patient	100 (86; 100)	50 (12; 88)	89 (71; 98)	100 (16; 100)	90	0.750	0.0253
	100 (86; 100)	*67 (22; 96)*	*92 (75; 99)*	*100 (29; 100)*	*93*	*0.833*	*0.0016*

Data from reader 1 (in upright) and from reader 2 (italicized) are given. If the p value < 0.05 (i.e., the AUC is significantly different from 0.5), there is evidence that the sequence does have an ability to detect lesions

In the per-patient analysis, which is the most critical assessment by the time of therapeutic decisions, the study showed that Acc of FSE was significantly higher than that of GE^{mDixon}. This may result from the combination of higher spatial resolution and more nuanced contrast resolution of FSE. The differences in Acc between the FSE and GE^{mDixon} ranged between 4% and 6%. The clinical relevance of these small differences should be studied more thoroughly.

Finally, our study demonstrated that the Fat sequence derived from the GE^{mDixon} provided higher contrast between lesion and reference tissue compared with FSE, reaching statistical significance for node metastases in all locations, and for bone metastases in the pelvis and thoracic spine. FSE images provided an intermediate contrast resolution between IP and Fat images.

Our study had several limitations. The results should be validated in a larger cohort of patients, to refine comparisons of the diagnostic value of the different sequences. Studies including patient from different centers should be performed to evaluate the importance of reader experience and of WB-MRI acquisitions on different magnets or with variations in acquisition parameters (field of view, acquisition planes, image resolution) [28]. The comparison of the performances of the different sequences was limited to FSE versus IP, Fat, and IP+Fat, respectively. This choice relies on a preliminary in-house experience and on previous studies comparing IP, OP, Fat, and Water images and showing that IP and Fat images were sufficient for the assessment of bone and node lesions [7, 18].

A non-isotropic 3D T1 GE Dixon sequence was used to reduce the sequence duration and allow breath-hold acquisitions. Although based on thicker imaging slices, the GE^{mDixon} provided satisfactory results in terms of contrast resolution, reproducibility of readings, and diagnostic performance. Increase in spatial resolution by moving towards isotropic millimetric sequences will most likely improve the value of this 3D T1 GE Dixon approach. This should be achievable,

Table 5 Comparison of the predictive accuracy (Acc) of MRI sequences in the per-organ (bone and nodes) and per-patient analyses

	FSE vs IP *p* value	FSE vs Fat *p* value	FSE vs all *p* value	IP vs Fat *p* value	IP vs all *p* value	Fat vs all *p* value
Bone	< 0.0001	0.6043	0.6043	< 0.0001	< 0.0001	1.0000
	FSE + 4.0%			Fat + 4.0%	All + 4.0%	
	< 0.0001	*< 0.0001*	*< 0.0001*	*0.5736*	*0.9798*	*0.6508*
	FSE + 4.0%	*FSE + 4.0%*	*FSE + 4.0%*			
Nodes	< 0.0001	< 0.0001	< 0.0001	< 0.0001	< 0.0001	1.0000
	IP + 4.0%	Fat + 6.0%	All + 6.0%	Fat + 4.0%	All + 4.0%	
	0.5047	*< 0.0001*	*< 0.0001*	*< 0.0001*	*< 0.0001*	*< 0.0001*
		Fat + 4.0%	*FSE + 1.0%*	*Fat + 4.0%*	*IP + 1.0%*	*Fat + 14%*
Per-patient	< 0.0001	< 0.0001	< 0.0001	< 0.0001	< 0.0001	1.0000
	FSE + 6.0%	FSE + 4.0%	FSE + 4.0%	Fat + 4.0%	All + 4.0%	
	< 0.0001	*< 0.0001*	*< 0.0001*	*< 0.0001*	*< 0.0001*	*0.6508*
	FSE + 6.0%	*FSE + 4.0%*	*FSE + 4.0%*	*Fat + 4.0%*	*All + 4.0%*	

Statistical differences are assessed following a resampling procedure, then *p* values and median differences in Acc (in %) from a Wilcoxon test are reported. Data from reader 1 (in upright) and from reader 2 (italicized) are given. The table reads as follows: in bone in reader 1, the accuracy of FSE is significantly higher (median difference + 4.0%, $p < 0.0001$) compared with that of IP, but not compared with that of Fat or of IP+Fat

thanks to the use of recent acceleration tools (compressed sensing) [29]. It is also worth mentioning that the total acquisition time may also be reduced if the combination of the Dixon method with a dual echo T2-weighted acquisition performs as well as the DWI sequence in detecting lesions [30].

Our study focused on morphologic sequences of WB-MRI studies in an homogeneous population of PCa patients. Future studies should compare FSE and GE^{mDixon} for lesion detection in other metastatic cancers, in multiple myeloma, and in lymphoma [7, 8]. Of note, WB-MRI examinations obtained for the follow-up of patients with testicular cancer already include mDixon images [31]. The benefit of mDixon sequences repeated after gadolinium injection for the detection of visceral metastasis should be studied, especially for cancers

Table 6 Contrast-to-reference ratio (CRR) for lesions in anatomic areas with metastases: median values are provided with the standard deviation in brackets

Anatomic area	FSE	IP	Fat	N^{lesion}	Difference in CRR
Skull	0.204	0.498	0.194	1	NC
Thoracic cage	0.157 (0.166)	0.201 (0.103)	0.095 (0.040)	3	NC
Cervical spine	0.219 (0.130)	0.432 (0.058)	0.082 (0.064)	2	NC
*Thoracic spine	0.246 (0.140)	0.352 (0.177)	0.137 (0.042)	10	†$^{FSE\ vs\ in\text{-}phase}$ $p = 0.0020$ †$^{FSE\ vs\ Fat}$ $p = 0.0137$
Lumbar spine	0.399 (0.059)	0.342 (0.165)	0.122 (0.125)	3	NC
*Pelvic	0.296 (0.113)	0.394 (0.141)	0.090 (0.071)	13	$^{FSE\ vs\ in\text{-}phase}$ $p = 0.0398$ †$^{FSE\ vs\ Fat}$ $p = 0.0002$
Humeral	0.348 (0.136)	0.365 (0.082)	0.050 (0.007)	2	NC
*Femoral	0.302 (0.128)	0.256 (0.168)	0.075 (0.070)	6	$^{FSE\ vs\ in\text{-}phase}$ $p = 0.4375$ $^{FSE\ vs\ Fat}$ $p = 0.0312$
*Lymph nodes	0.332 (0.076)	0.400 (0.130)	0.065 (0.043)	18	$^{FSE\ vs\ in\text{-}phase}$ $p = 0.0432$ †$^{FSE\ vs\ Fat}$ $p < 0.0001$

A low CRR indicates a high contrast between lesion and reference tissue. According to the Wilcoxon test, the difference in CRR between FSE and Dixon sequences was statistically significant in thoracic spine, bony pelvis, and lymph nodes (the Fat sequence yielding a higher contrast between lesion and reference tissue compared to FSE)

NC, non-computable due to the low number of positive lesions

*Significant Kruskal-Wallis test

† Significant Wilcoxon test

prone to metastasize to the liver or brain. In bones, these post-contrast sequences have shown no added value compared with non-contrast 3D T1 GE images and DWI for the diagnosis of bone metastases in PCa [8].

In conclusion, this study compared the image contrast, reproducibility, and diagnostic performance of 3D T1 FSE and 3D T1 GE^{mDixon} sequences obtained as morphologic sequences complementing DWI to detect bone and node metastasis in PCa. The use of GE^{mDixon} instead of FSE would reduce the acquisition time of the 3D T1 sequence by more than 10 min, bringing the perspective of WB-MRI examinations obtained in less than 20 min. The Fat sequence derived from GE^{mDixon} yielded best contrast between lesion and reference tissue. A similar reproducibility of readings was found for FSE and GE^{mDixon}. Differences in predictive accuracy in detecting metastases ranged from + 4% to + 6% in favor of GE^{mDixon} (nodes) to + 4% to + 6% in favor of FSE (bone and patient staging).

Funding Information The authors state that this work has not received any funding.

Compliance with ethical standards

Guarantor The scientific guarantor of this publication is F.E. Lecouvet.

Conflict of interest One of the authors of this manuscript (Vincent Denolin) was an employee of Philips Medical Systems International at the time of this study. The remaining authors declare no relationships with any companies whose products or services may be related to the subject matter of the article.

Statistics and biometry One of the authors has significant statistical expertise (N. Michoux).

Informed consent Written informed consent was obtained from all subjects (patients) in this study.

Ethical approval Institutional Review Board approval was obtained.

Study subjects or cohorts overlap Study subjects or cohorts have not been previously reported.

Methodology
- Prospective
- Diagnostic or prognostic study
- Performed at one institution

References

1. Steinborn MM, Heuck AF, Tiling R, Bruegel M, Gauger L, Reiser MF (1999) Whole-body bone marrow MRI in patients with metastatic disease to the skeletal system. J Comput Assist Tomogr 23:123–129
2. Lecouvet FE (2016) Whole-body MR imaging: musculoskeletal applications. Radiology 279:345–365
3. Pasoglou V, Michoux N, Tombal B, Jamar F, Lecouvet FE (2015) WbMRI to detect bone metastases: critical review on diagnostic accuracy and comparison to other imaging modalities. Clin Transl Imaging 3:141–157
4. Padhani AR, Lecouvet FE, Tunariu N et al (2017) Metastasis reporting and data system for prostate cancer: practical guidelines for acquisition, interpretation, and reporting of whole-body magnetic resonance imaging-based evaluations of multiorgan involvement in advanced prostate cancer. Eur Urol 71:81–92
5. Pasoglou V, Michoux N, Peeters F et al (2015) Whole-body 3D T1-weighted MR imaging in patients with prostate cancer: feasibility and evaluation in screening for metastatic disease. Radiology 275:155–166
6. Padhani AR, Lecouvet FE, Tunariu N et al (2017) Rationale for modernising imaging in advanced prostate cancer. Eur Urol Focus 3:223–239
7. Bray TJP, Singh S, Latifoltojar A et al (2017) Diagnostic utility of whole body Dixon MRI in multiple myeloma: a multi-reader study. PLoS One 12:e0180562
8. Johnston EW, Latifoltojar A, Sidhu HS et al (2018) Multiparametric whole-body 3.0-T MRI in newly diagnosed intermediate- and high-risk prostate cancer: diagnostic accuracy and interobserver agreement for nodal and metastatic staging. Eur Radiol 29(6):3159–3169. https://doi.org/10.1007/s00330-018-5813-4
9. Guerini H, Omoumi P, Guichoux F et al (2015) Fat suppression with Dixon techniques in musculoskeletal magnetic resonance imaging: a pictorial review. Semin Musculoskelet Radiol 19:335–347
10. Rambow O, Hazle J, Clark J, Ma J (2013) Direct water and fat determination in two-point Dixon imaging with flexible echo times. Med Phys 40:112302
11. Larbi A, Omoumi P, Pasoglou V et al (2018) Whole-body MRI to assess bone involvement in prostate cancer and multiple myeloma: comparison of the diagnostic accuracies of the T1, short tau inversion recovery (STIR), and high b-values diffusion-weighted imaging (DWI) sequences. Eur Radiol 29(8):4503–4513. https://doi.org/10.1007/s00330-018-5796-1
12. Widmann G, Henninger B, Kremser C, Jaschke W (2017) MRI sequences in head & neck radiology - state of the art. Rofo 189:413–422
13. Metser U, Chan R, Veit-Haibach P, Ghai S, Tau N (2019) Comparison of MRI sequences in whole-body PET/MRI for staging of patients with high-risk prostate cancer. AJR Am J Roentgenol 212:377–381
14. Bastian PJ, Boorjian SA, Bossi A et al (2012) High-risk prostate cancer: from definition to contemporary management. Eur Urol 61:1096–1106
15. Heidenreich A, Bastian PJ, Bellmunt J et al (2014) EAU guidelines on prostate cancer. Part II: Treatment of advanced, relapsing, and castration-resistant prostate cancer. Eur Urol 65:467–479
16. Barentsz JO, Weinreb JC, Verma S et al (2016) Synopsis of the PI-RADS v2 guidelines for multiparametric prostate magnetic resonance imaging and recommendations for use. Eur Urol 69:41–49
17. Eggers H, Brendel B, Duijndam A, Herigault G (2011) Dual-echo Dixon imaging with flexible choice of echo times. Magn Reson Med 65:96–107
18. Costelloe CM, Madewell JE, Kundra V, Harrell RK, Bassett RL Jr, Ma J (2013) Conspicuity of bone metastases on fast Dixon-based multisequence whole-body MRI: clinical utility per sequence. Magn Reson Imaging 31:669–675
19. Scott WA (1955) Reliability of content analysis: the case of nominal scale coding. Public Opin Q:321–325
20. Maeder Y, Dunet V, Richard R, Becce F, Omoumi P (2018) Bone marrow metastases: T2-weighted Dixon spin-echo fat images can replace T1-weighted spin-echo images. Radiology 286:948–959
21. Lecouvet FE, Geukens D, Stainier A et al (2007) Magnetic resonance imaging of the axial skeleton for detecting bone metastases in

patients with high-risk prostate cancer: diagnostic and cost-effectiveness and comparison with current detection strategies. J Clin Oncol 25:3281–3287
22. Zweig MH, Campbell G (1993) Receiver-operating characteristic (ROC) plots: a fundamental evaluation tool in clinical medicine. Clin Chem 39:561–577
23. Curran-Everett D (2000) Multiple comparisons: philosophies and illustrations. Am J Physiol Regul Integr Comp Physiol 279:R1–R8
24. Messiou C, Hillengass J, Delorme S et al (2019) Guidelines for acquisition, interpretation, and reporting of whole-body MRI in myeloma: Myeloma Response Assessment and Diagnosis System (MY-RADS). Radiology 291:5–13
25. Park HJ, Lee SY, Rho MH et al (2016) Usefulness of the fast spin-echo three-point Dixon (mDixon) image of the knee joint on 3.0-T MRI: comparison with conventional fast spin-echo T2 weighted image. Br J Radiol 89:20151074
26. Gaddikeri S, Mossa-Basha M, Andre JB, Hippe DS, Anzai Y (2018) Optimal fat suppression in head and neck MRI: comparison of multipoint Dixon with 2 different fat-suppression techniques, spectral presaturation and inversion recovery, and STIR. AJNR Am J Neuroradiol 39:362–368
27. Samji K, Alrashed A, Shabana WM, McInnes MD, Bayram E, Schieda N (2016) Comparison of high-resolution T1W 3D GRE (LAVA) with 2-point Dixon fat/water separation (FLEX) to T1W fast spin echo (FSE) in prostate cancer (PCa). Clin Imaging 40: 407–413
28. Kochanek KD, Murphy SL, Xu J, Tejada-Vera B (2016) Deaths: final data for 2014. Natl Vital Stat Rep 65:1–122
29. Nam JG, Lee JM, Lee SM et al (2019) High acceleration three-dimensional T1-weighted dual echo Dixon hepatobiliary phase imaging using compressed sensing-sensitivity encoding: comparison of image quality and solid lesion detectability with the standard T1-weighted sequence. Korean J Radiol 20:438–448
30. Wang X, Pirasteh A, Brugarolas J et al (2018) Whole-body MRI for metastatic cancer detection using T2 -weighted imaging with fat and fluid suppression. Magn Reson Med 80:1402–1415
31. Mosavi F, Laurell A, Ahlstrom H (2015) Whole body MRI, including diffusion-weighted imaging in follow-up of patients with testicular cancer. Acta Oncol 54:1763–1769